Applied Catalysis B: Environmental 160–161 (2014) 423–435

Contents lists available at ScienceDirect

Applied Catalysis B: Environmental

journal homepage: www.elsevier.com/locate/apcatb

Identification of bimetallic electrocatalysts for ethanol and acetaldehyde oxidation: Probing C_2-pathway and activity for hydrogen oxidation for indirect hydrogen fuel cells

A.C. Queiroz [a], W.O. Silva [b], I.A. Rodrigues [b], F.H.B. Lima [a,*]

[a] Instituto de Química de São Carlos, Universidade de São Paulo, CEP 13560-970, CP 780 São Carlos, SP, Brazil
[b] Departamento de Química, Universidade Federal do Maranhão, CEP 65080-040, São Luiz, MA, Brazil

ARTICLE INFO

Article history:
Received 29 December 2013
Received in revised form 23 May 2014
Accepted 30 May 2014
Available online 6 June 2014

Keywords:
Ethanol electro-oxidation
HOR
On-line DEMS
Selective electro-oxidation
Bimetallic electrocatalysts
Indirect hydrogen fuel cells

ABSTRACT

Hydrogen, in the ethanol molecule, can be utilized in indirect hydrogen fuel cells. In this device, ethanol can be dehydrogenated producing H_2 and acetaldehyde in an external fuel processor, and the H_2 molecules are electro-oxidized in the anode. The anode electrocatalyst can, additionally, be active for the electro-oxidation of residual ethanol or acetaldehyde, but must catalyze the reaction *via* the C_2-pathway (intact C—C bond), in order to avoid the formation poisoning species. This work investigated potential materials that are active for H_2 and catalyze the selective electro-oxidation of ethanol and acetaldehyde *via* the C_2-pathway. The bimetallic electrocatalysts were formed by W, Ru and Sn-modified Pt nanoparticles. The reaction products were followed by on-line differential electrochemical mass spectrometry (DEMS) experiments. The results showed that Ru/Pt/C and Sn/Pt/C presented higher overall reaction rate when compared to the other studied materials. However, they were non-selective, even at different atomic proportions, and catalyzed the reaction in parallel pathways producing CO_2 and acetaldehyde, with Ru/Pt/C presenting the highest average current efficiency for CO_2 formation (16.6%). On the other hand, W/Pt/C with high W content was more selective to the C_2 route, evidenced by the absence of the DEMS signals for molecules with one carbon atom such as CH_4 and CO_2. Additionally, this material was active and stable for H_2 electro-oxidation, even in the presence of acetaldehyde in solution, contrarily to what was observed for Pt/C, and this was associated to its activity for H_2 oxidation and its inability for the C—C dissociation, as evidenced by the DEMS measurements. The high selectivity obtained for the W/Pt/C material to the C_2-pathway, and its capability for hydrogen electro-oxidation, is an important novelty in this work, as it turns into a potential electrocatalyst for application in the anode of indirect hydrogen fuel cells powered by ethanol, mainly for those that operates as auxiliary power units of internal combustion engine cars.

1. Introduction

Hydrogen is considered a clean and environmental friendly energy carrier. This fuel can be stored in liquid or gaseous form, as proposed before [1–3]. Inorganic or organic molecules with a high content of hydrogen atoms can be considered as hydrogen "reservoirs", offering the possibility of using them with the existing fuel infrastructure [4,5]. These compounds can be produced by hydrogenation *via* heterogeneous chemical catalysis, electrochemical reduction, and by biochemical routes, as in the case of the bioethanol. In the particular case of regenerative hydrogenation/dehydrogenation cycles, the conversion reactions can be performed by catalytic thermal hydrogenation/dehydrogenation or by electrochemical reduction/oxidation. In the last case, the hydrogenation is achieved by electrochemical reduction of an oxidized molecule, and the dehydrogenation (H_2 production) can be accomplished by electrochemical reforming [6,7]. In the case of being organic molecules, as discussed before [8–10], these materials can be called "organic chemical hydrides", because they can freely "absorb" and "desorb" hydrogen like metal hydrides by catalytic reactions.

In order to efficiently utilize the stored hydrogen, an important manner is to use the molecule to feed a fuel cell. Fuel cells convert chemical energy from a fuel into electric energy. These devices are important mainly due to their high theoretical conversion efficiency [11]. Moreover, fuel cells have a broad variety

* Corresponding author. Tel.: +55 16 3373 8681; fax: +55 16 3373 9952.
E-mail addresses: fabiohbl@iqsc.usp.br, fabiohbl@gmail.com (F.H.B. Lima).

http://dx.doi.org/10.1016/j.apcatb.2014.05.055
0926-3373/

of application, ranging from the use in portable electronic devices to the use as electric energy backup for industrial or commercial buildings. Basically, there are two main types of fuel cells that can be used to feed with hydrogenated or "reduced" molecules: (i) indirect hydrogen fuel cells: in this case, the hydrogenated molecule is submitted to a thermal catalytic dehydrogenation, in an external fuel processor, and the released H_2 and by-products, is used to fed to a conventional PEM (polymer electrolyte membrane) hydrogen fuel cell [12–15]; (ii) direct fuel cells or "virtual hydrogen" fuel cells [16–18]: in this case, instead of releasing hydrogen gas, this step can be replaced by an electrochemical oxidation step, which releases protons and electrons [8]. For the last case, the fuel cells can operate in two regimes: (i) as a rechargeable or regenerative fuel cell, which uses a reversible electrochemical hydrogenation/dehydrogenation cycle of a particular organic molecule [19], and (ii) as non-electrochemical rechargeable or non-regenerative device, in which the fuel is electrochemical and irreversibly oxidized into a molecule, such as CO_2.

Among the studied fuels for non-regenerative fuel cells, ethanol has come to prominence, mainly due to its high hydrogen content or high energy density, low toxicity, and possibility to be produced in large amounts through the fermentation of biomass, offering an interesting economic viability. Ethanol can be used in indirect or direct fuel cells (direct ethanol fuel cell – DEFC) [18]. Thus, in the former case, the anode electrocatalyst has to be active for the H_2 electro-oxidations (HOR) and tolerant (inactive) to the presence of the dehydrogenation by-products, such as acetaldehyde and, eventually, unreacted ethanol.

For DEFC, at low temperature (virtual hydrogen fuel cells), the electrocatalysts ought to be high efficient for the electro-oxidation of ethanol to CO_2. The total electro-oxidation of ethanol to CO_2 releases 12 electrons per molecule ($CH_3CH_2OH + 3H_2O = 2CO_2 + 12H^+ + 12e^-$). As proposed before by Lai and co-authors [20] there are two main routes for the ethanol electro-oxidation reaction: the C_2 and C_1-pathways: in the C_1-pathway, the carbon-carbon bond can be broken in ethanol or acetaldehyde, at low potentials, producing CO_{ad} and CH_x-species, which, eventually, oxidizes to carbon dioxide [21,22]. In the C_2-pathway, the carbon–carbon bond of ethanol remains intact upon oxidation, and it is converted to acetaldehyde and, eventually, upon further oxidation, to acetic acid. Platinum is the most active monometallic electrocatalyst, but it presents very low Faradaic efficiency for CO_2 formation [23,24]. Several studies using bi and trimetallic electrocatalysts have shown an increased in the overall reaction rate, but, up to now, the obtained Faradaic current efficiencies for CO_2 formation (or C1-pathway) are insufficient (lower than 5%) for the development of practical PEM DEFC systems [24–29,20,30–32,21,22,33–37].

On the other hand, the use of ethanol in fuel cells with external fuel processors (indirect hydrogen fuel cells), is becoming attractive. In these devices, ethanol can be dehydrogenated in the fuel processor, and the resulting stream, containing H_2, acetaldehyde and, possibly, unreacted ethanol, is used to feed the fuel cell anode. Therefore, the anode electrocatalyst has to be active for H_2 electro-oxidation and, additionally, can be active for the electro-oxidation of residual ethanol or acetaldehyde, which will contribute to increase the overall Faradaic current (in the C_2-pathway, ethanol to acetaldehyde or acetic acid, and acetaldehyde to acetic acid). However, if active, the electrocatalyst must catalyzed the ethanol or acetaldehyde electro-oxidation *via* the C_2-pathway (intact C—C bond), in order to avoid the formation adsorbed poisoning species with 1-carbon atom, such as CO and CH_x, that cannot be oxidized at low potentials. This fuel cell could be used, for example, as an auxiliary power unit of internal combustion engine cars, powered by ethanol. In this scenario, part of the ethanol could be used in order to power the fuel cell, generating electricity, and the non-used dehydrogenation by-product (or residual ethanol) could be pumped back to the ethanol tank for additional combustion. This would be, therefore, a significant innovation concerning practical application of fuel cells. The attempt for the search of electrocatalysts that selectively oxidizes ethanol or acetaldehyde *via* the C_2-pathway and, furthermore, active for molecular hydrogen electro-oxidation, is new in the literature. Thus, investigations in this direction are very important for the development of indirect hydrogen fuel cells.

Therefore, the aim of this work is related to the investigation of potential materials that are active for the electro-oxidation of ethanol and acetaldehyde *via* the C_2-pathway, and active for the electro-oxidation of molecular hydrogen. The investigated materials were formed by bimetallic nanoparticles composed of Pt in combination with Sn, Ru and W atoms. It was investigated the correlation electrocatalyst composition-reaction product distribution using on-line differential electrochemical mass spectrometry (DEMS). Additionally, it was investigated the electro-oxidation of hydrogen in the absence and in the presence of acetaldehyde, catalyzed by the most selective material for the C_2-pathway.

2. Experimental

2.1. Synthesis and characterization of the nanoparticles

The electrocatalysts were formed by carbon-supported Ru, Sn and W-modified Pt nanoparticles, represented by Ru/Pt/C, Sn/Pt/C and W/Pt/C, respectively (alloy or solid solution-depending on the metal combination). The electrocatalysts were synthesized with nominal atomic ratios (metal:Pt) of 1:3 and 2:3, adapting a previously published method [38]. For the synthesis, appropriate amounts of $RuCl_2$, $SnCl_2$ or WCl_6 (being WCl_6 initially solubilized in 25 mL of a solution NaOH 0.1 mol L^{-1}) and $H_2PtCl_2{\cdot}6H_2O$ (Sigma–Aldrich) were solubilized in ultrapure water, followed by the addition of high surface area carbon (Vulcan XC-72, Cabot, 250 $m^2\,g^{-1}$). The resulting suspension was stirred and sonicated for 10 min in air at room temperature. After this, the solution was stirred and heated at 80 °C until complete evaporation of the solvent in a Petri dish. The samples were cooled in air, and the impregnated powders were submitted to thermal treatment, conducted in a tubular oven (MAITEC) under argon atmosphere at 300 °C, for 1 h, followed by treatment under H_2 atmosphere at 300 °C for 3 h. After this, all samples were filtered, washed with ultrapure water, and dried at 70 °C in a conventional oven during 24 h.

The resulting electrocatalyst atomic compositions were estimated by X-ray energy dispersive spectroscopy (X-EDS) analysis, using a Zeiss-Leica/LEO 440 model (LEO, UK) scanning electron microscopy (SEM) with a Link Analytical micro-analyzer (Isis System Series 200). The distribution of the metal nanoparticles on the carbon powder support and the particle sizes were investigated by measurements of Transmission Electron Microscopy (TEM), using a Jeol 2010 microscope, bearing a LaB_6 filament and operated at 200 kV accelerating voltage. The samples were prepared by ultrasonically treating the catalyst powders in isopropyl alcohol. A drop of the resulting dispersion was placed on thin carbon films deposited on standard TEM copper grids and dried in air. The images were acquired by observing many different areas of the samples, in order to assess its average characteristics. The diameters of the catalyst particles were measured from the TEM images using the *ImageJ* software. At least 500 nanoparticles of each sample were measured to build the size distribution histograms. Structural features were also investigated by X-ray diffraction (XRD) measurements, carried out using a RIGAKU Ultima IV diffractometer with Cu K_α radiation (λ = 1.54056 Å), operated at 40 kV and 40 mA, and between 20° and

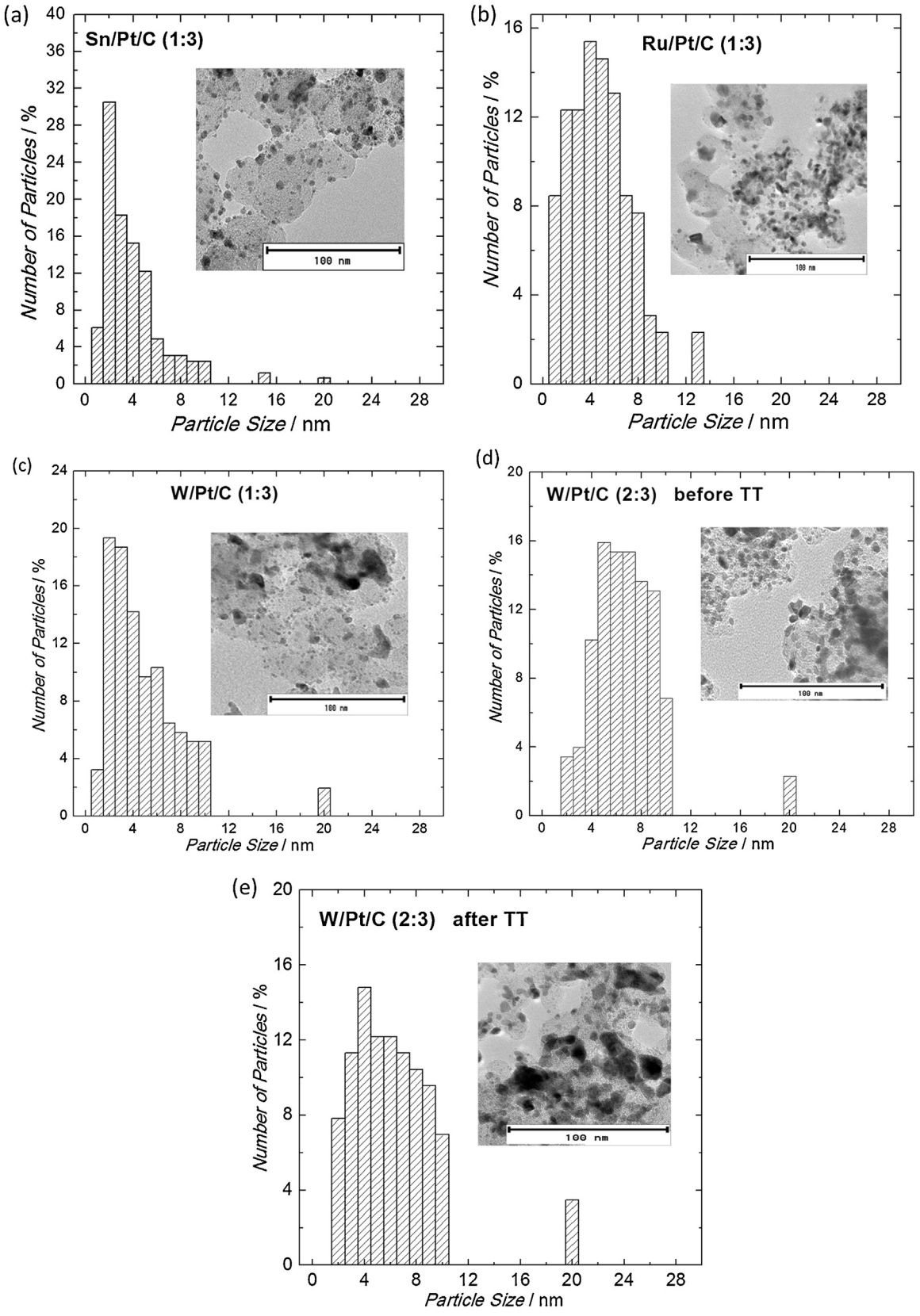

Fig. 1. TEM images and particle size distribution histograms for the different carbon-supported nanoparticles: (a) Sn/Pt/C (1:3); (b) Ru/Pt/C (1:3); (c) W/Pt/C (1:3); (d) W/Pt/C (2:3) before thermal treatment; (e) W/Pt/C (2:3) after thermal treatment.

Table 1
Electrocatalyst structural features obtained by X-ray energy dispersive spectroscopy, X-ray diffraction experiments, and transmission electron microscopy.

Electrocatalyst	EDS (Pt atomic composition) (%)	EDS (metal atomic composition) (%)	XRD (lattice parameter) (nm)	XRD (average crystallite size) (nm)	TEM (average particle size) (nm)
Sn/Pt/C (1:3)	78.2	21.7	0.3926	8.6	3.0
Ru/Pt/C (1:3)	80.1	19.8	0.3911	11.8	4.5
W/Pt/C (1:3)	80.9	19.0	0.3922	21.3	4.5
W/Pt/C (2:3)	63.1	36.8	0.3922	30.0	5.0
Pt/C	–	–	0.3923	2.8	2.5

100°, with a scan rate of 0.3° min^{-1}. The average crystallite sizes were estimated from the (1 1 1) peak of the Pt diffraction pattern, using the Scherrer equation [39].

2.2. Electrochemical experiments

Electrochemical measurements of cyclic voltammetry and chronoamperometry were performed using an Autolab PGSTAT 30 equipped with an analog Scangen module. All experiments were conducted in 0.5 mol L^{-1} H_2SO_4 electrolyte, prepared from high purity reagents (Sigma–Aldrich) and water purified in a Milli-Q (Millipore) system, under controlled temperature of 25 ± 0.1 °C using a Hakee-K20 thermostat. A ring-shaped platinized platinum foil served as counter and a reversible hydrogen electrode (RHE), in the same electrolyte, was used as reference electrode. The electrochemical oxidation of ethanol or acetaldehyde was carried out using the DEMS electrode (Section 2.3) in 0.1 mol L^{-1} CH_3CH_2OH or CH_3CHO/0.5 mol L^{-1} H_2SO_4 solution. The electrochemical oxidation of hydrogen was measured using a rotating disk electrode (RDE) in H_2-saturated 0.5 mol L^{-1} H_2SO_4 electrolyte at 1600 rpm. For the RDE, a suspension of 2.0 mg mL^{-1} of the metal/C was prepared, dispersing the catalyst powder in isopropyl alcohol using an ultrasound bath [40]. A 20 μL aliquot of the dispersed suspension was pipetted onto the top of a glassy carbon disk of a rotating disk electrode (RDE) (5 mm diameter, 0.196 cm^2) and dried under vacuum, resulting in 40 μg_{metal} cm^{-2}.

2.3. Differential electrochemical mass spectrometry (DEMS) setup

On-line DEMS measurements were performed with a Pfeiffer Vacuum QMA 200 quadrupole mass spectrometer using a setup consisting of two differentially pumping chambers. More details and features of this method are presented in previous publications [41,42]. This technique allows the on-line detection of volatile and gaseous products of electrochemical reactions during the application of a potential scan. The electrochemical cell was constructed following previously published principles [41,43]. In the experiments of this work, the current *versus* potential curves were recorded simultaneously with the mass intensity *versus* potential curves, for selected values of m/z (mass/charge) ionic signals. The electrode potential was cycled in the range of 0.05–1.0 V for bimetallic materials and between 0.05 and 1.2 V for Pt/C, all with a scan rate of 0.01 V s^{-1}.

For the DEMS measurements, the working electrodes were prepared in the form of a thin film by pippeting a total of 180 μL of an aqueous suspension of the electrocatalyst (2.0 mg mL^{-1} in 1.0 mL of isopropyl alcohol + 50 μL of Nafion® solution–5 wt.%, Aldrich) [40] onto a gold layer (1.13 cm^2 area, 50 nm thickness), obtained by Au sputtering onto a Gore-Tex® PTFE membrane (pore size 0.02 μm), resulting in 120 μg_{metal} cm^{-2}. After the evaporation of the alcohol at ambient temperature, the electrodes were washed with ultrapure water and inserted in the DEMS electrochemical cell.

The ethanol electro-oxidation productions were monitored at m/z = 22 (CO_2: doubly ionized – CO_2^{2+}), m/z = 29 (acetaldehyde), and m/z = 44 (acetaldehyde + CO_2) [44–46]. Quantitative analysis of the DEMS measurements was performed following a previous procedure [23]. Accordingly, the average current efficiency for complete ethanol electro-oxidation to CO_2 per one carbon atom (12 electrons per ethanol molecule) was calculated using the following equation:

$$A_q(CO_2) = \frac{6Q_i}{K^*_{22}Q_f}$$

or

$$A_i(CO_2) = \frac{6I_i}{K^*_{22}I_f}$$

In which Q_f and I_f are the Faradaic charge and Faradaic current during ethanol oxidation, respectively, and Q_i and I_i are the corresponding mass spectrometric charge and current of m/z = 22; the factor 6 refers to the number of electrons needed for the formation of one CO_2 molecule from ethanol, and K^*_{22} is the calibration

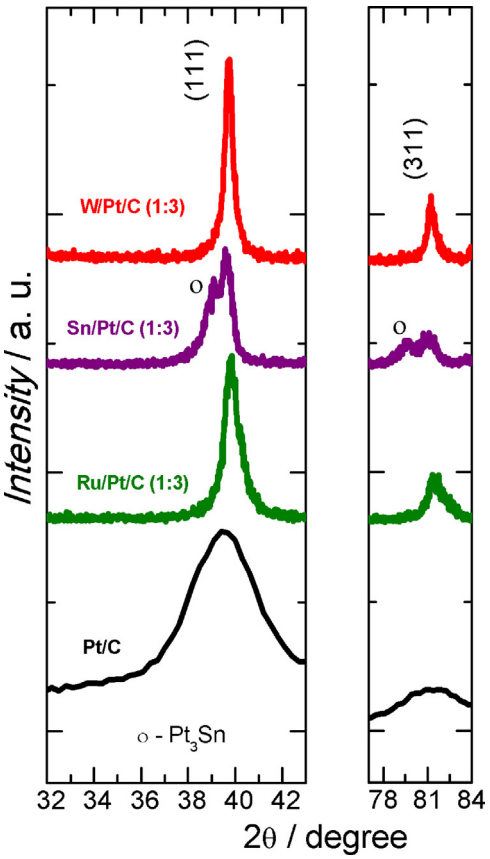

Fig. 2. X-ray powder diffraction intensities for the as-prepared nanoparticles (a) W/Pt/C (1:3), (b) Sn/Pt/C (1:3) and (c) Ru/Pt/C (1:3). The spectra obtained for Pt/C is included for comparison.

constant for $m/z = 22$ determined from CO_{ad} oxidation (CO stripping) or CO bulk oxidation on a Pt catalyst. For CO_{ad} oxidation and CO bulk oxidation, respectively, K^*_{22} was calculated by:

$$K^*_{22} = \frac{2Q_i}{Q_f}$$

or

$$K^*_{22} = \frac{2I_i}{I_f}$$

In which Q_f and I_f are the Faradaic charge and the Faradaic current during CO_{ad} oxidation and CO bulk oxidation, respectively, and Q_i and I_i are the corresponding mass spectrometric charge and current of $m/z = 22$. The factor 2 refers to the number of electrons needed for formation of one CO_2 molecule from CO_{ad} or bulk CO. For the CO stripping experiments, the CO saturation coverage on the electrocatalyst surface was achieved by bubbling CO in the solution for 10 min with the electrode polarized at 0.1 V, followed by bubbling N_2 for 30 min in order to eliminate dissolved CO [47].

3. Results and discussion

3.1. Nanoparticles characterization

The electrocatalyst atomic compositions of the as-prepared nanoparticles were estimated by X-EDS measurements, and the results are presented in Table 1. The results showed that the atomic ratios were close to 1:4 (metal:platinum), instead of the 1:3 nominal values. For W/Pt/C, with higher amount of W, however, the result was closer to the nominal value of 2:3. These differences in the obtained atomic ratios may arise from the hydration of the precursor metal salts, which interferes the weight values during the synthesis.

The TEM images and the particle diameter distribution histograms obtained for the different investigated materials are presented in Fig. 1. The images reveal uniform distribution of the metal nanoparticles on the carbon powder support, but with heterogeneous distribution in size. According to the obtained histograms, the three different materials with 1:3 atomic ratios presented average particle size in the range of 2–10 nm, and some large particle agglomerates in the range of 12–20 nm. The effect of the thermal treatment was also investigated, and the TEM results of W/Pt/C (2:3) before and after thermal treatment under H_2 atmosphere at 300 °C are shown in Fig. 1(d) and (e), respectively. As can be observed, there is only a marginal change in the particle size distribution histogram (from *ca.* 4.5 to 5.0 nm), indicating that the thermal treatment involved in the synthesis procedure does not have a severe effect on increasing the electrocatalyst particle size.

The X-ray diffraction patterns obtained for the (1 1 1) and (3 1 1) planes for the synthesized Ru/Pt/C, Sn/Pt/C and W/Pt/C materials are presented in Fig. 2. The result for Pt/C nanoparticles

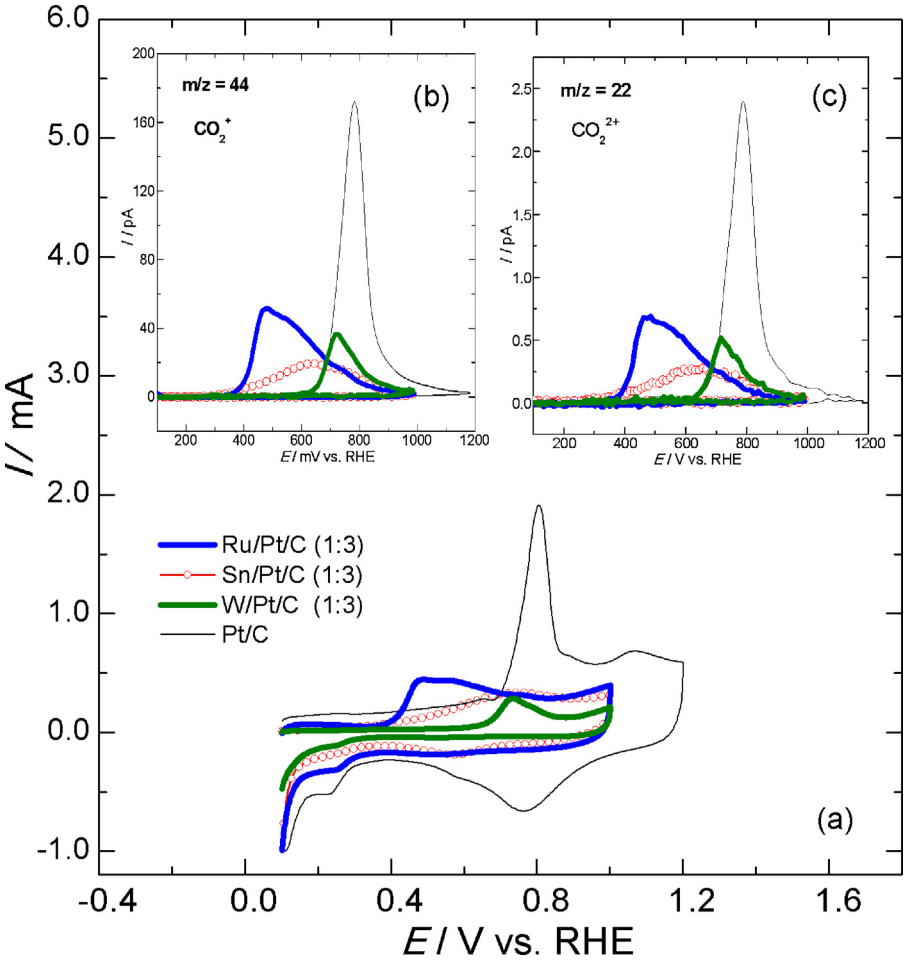

Fig. 3. Faradaic (a) and ionic currents for $m/z = 44$ (CO_2, CO_2^+) (b) and $m/z = 22$ (CO_2, CO_2^{2+}) (c) obtained during DEMS experiments of hold-scan for CO stripping on the different investigated electrocatalysts, in 0.5 mol L^{-1} H_2SO_4 electrolyte at 25 °C. Potential was hold at 0.1 V, during 10 min, in CO-saturated solution, and the CV was obtained at scan rate of 10 mV s^{-1}, after saturating the solution with argon, during 20 min.

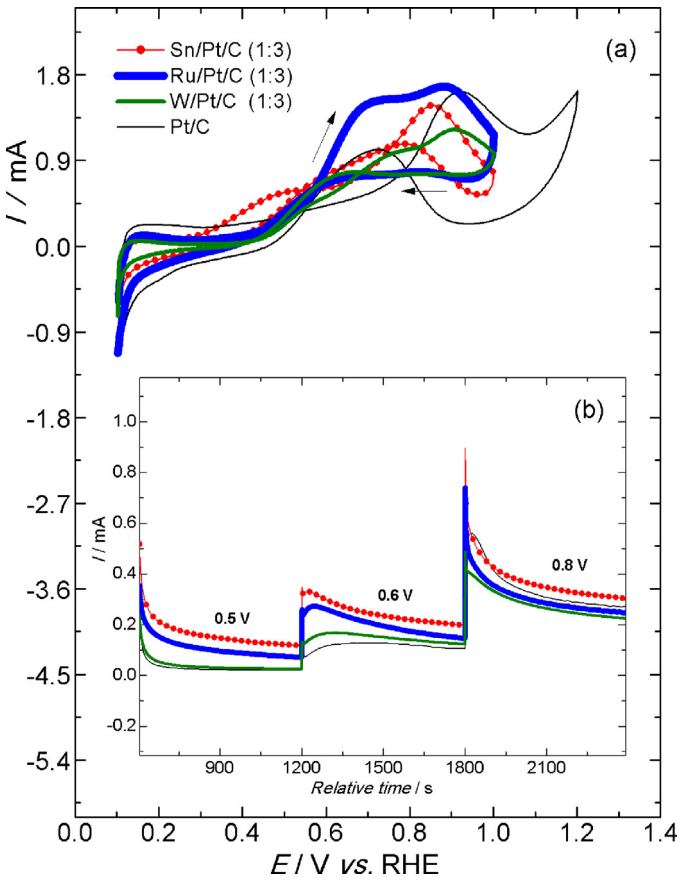

Fig. 4. Faradaic currents obtained during (a) cyclic voltammetry and (b) chronoamperometry in DEMS measurements of ethanol electro-oxidation catalyzed by investigated electrocatalysts in 0.1 mol L^{-1} C_2H_5OH and 0.5 mol L^{-1} H_2SO_4 solution at 25 °C. The CV measurements were conducted at a scan rate of 10 mV s^{-1} and the chronoamperometric curves were performed with a multiple potential jump procedure, with the currents being registered during 10 min.

was included for comparison. These patterns are related to the face-centered cubic (fcc) crystalline structure of Pt. As can be observed, the diffraction peaks are only slight shifted to higher angles with respect to those of the Pt/C electrocatalyst. This indicates low degree of alloy formation. In fact, the calculated lattice parameters, presented in Table 1, show very low lattice change, evidencing low insertion of Ru, Sn or W atoms into the Pt lattice. In the case of the Sn/Pt/C material, it is clearly observed additional reflections, as marked in the figure, indicating the formation of a defined Pt_3Sn alloy phase, with a higher lattice parameter value (0.3996 nm), due to the large size of Sn, when compared to that of Pt atoms. However, this is present as a minor phase, as indirectly evidenced by the low intensity of these diffraction peaks. Therefore, it can be inferred that the major part of the electrocatalyst is formed by segregated phases, but with a close contact of the components, and with low insertion of Ru, Sn or W atoms into the Pt lattice.

Additionally, sharper diffraction peaks are observed for the bimetallic materials, while those of the Pt/C are broader. Actually, the average crystallite sizes, estimated using the Sherrer equation, also presented in Table 1, resulted in larger crystallites for the bimetallic materials, when compared to that of Pt/C. The larger crystallite size of the bimetallic materials may be ascribed to adopted synthesis method. Furthermore, it is noted larger crystallites for the materials with W atoms, which may indicate higher susceptibility for growth during the synthesis. It is worth noting that the calculated values of crystallite sizes are higher than the average particle sizes obtained by TEM. This is ascribed to the major contribution of the larger crystallites, present in all investigated material, to the diffraction intensity and, so, resulting in high values of crystallite sizes, as calculated using the Scherrer equation.

3.2. DEMS experiments of ethanol electro-oxidation catalyzed by Ru/Pt/C, Sn/Pt/C and W/Pt/C

Fig. 3(a) shows the currents of adsorbed CO oxidation (CO stripping), and Fig. 3(b) and (c) shows the ionic signals $m/z = 44$ and $m/z = 22$, respectively, both corresponding to the CO_2 formation. Lower CO oxidation overpotential is observed for the materials with Ru and Sn, which is a consequence of the facilitated CO oxidation on Ru or Sn-containing materials. This can be explained by the bi-functional mechanism, in which the Ru or Sn atoms provide oxygenated species for the CO—O coupling, as proposed before [48]. In the case of the W/Pt/C material, it is also seen a negative shift of the onset potential for the CO oxidation compared to Pt/C. However, this shift is not as pronounced as those observed for the Ru or Sn-containing electrocatalyst. So, it seems that the formation of "active" oxygenated species on W, necessary for the oxidation of CO, takes place at a lower extent [49,50]. In all cases, the CO_2 ionic signals, measured by DEMS, match with the Faradaic current profiles, being better for the onset potential determination, because the ionic current signals are free from the double layer charging phenomenon. It is worth noting that the peaks for the CO electro-oxidation on the Ru/Pt/C (1:3) and Sn/Pt/C (1:3) materials are broader than that for Pt/C. This may be attributed to the presence crystallites with different sizes for the bimetallic materials. Smaller crystallites have high lying d-band center, leading to

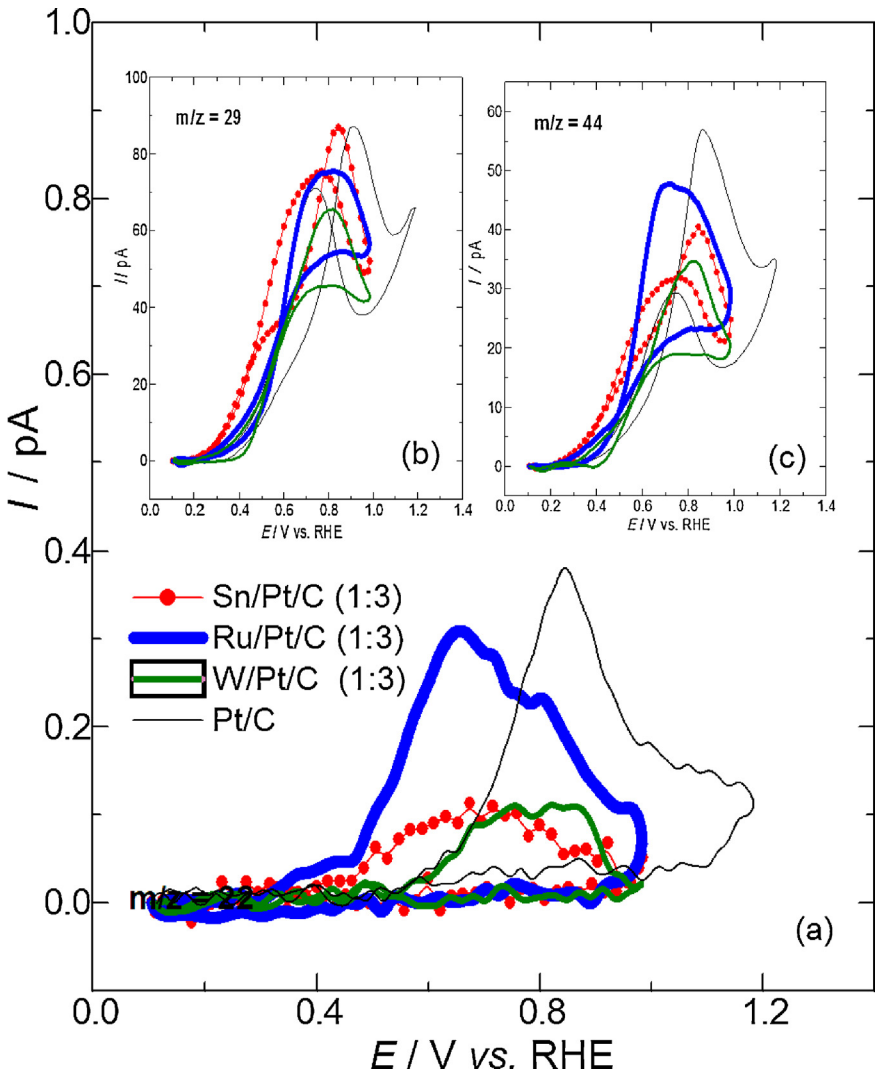

Fig. 5. Ionic currents obtained in DEMS experiments during CV of ethanol electro-oxidation reaction catalyzed by the different investigated electrocatalysts: (a) $m/z = 22$ (CO_2^{2+}); (b) $m/z = 29$ (acetaldehyde, CHO^+), and (c) $m/z = 44$ (CO_2, CO_2^+ + acetaldehyde, CH_3CHO^+) in 0.1 mol L^{-1} ethanol and in 0.5 mol L^{-1} H_2SO_4 electrolyte at 25 °C. Scan rate of 10 mV s^{-1}.

a stronger metal–CO adsorption, which decreases the CO oxidation rate at lower potentials. Larger crystallites possess lower lying d-band center, which conducts to a weaker metal–CO adsorption, and so, a facilitated the CO stripping at lower potentials. Crystallites with different sizes also have different overall number of defects, which influences the activity for water activation (forming adsorbed oxygenated species), necessary for the CO—O coupling. Additionally, this broad feature can also be a consequence of a non-homogeneous value for the distance between Pt and Ru or Sn active sites, which affect the CO electro-oxidation. All these variables may have an important contribution influencing the electro-oxidation rate of adsorbed CO, producing a broad current peak as a function of the potential.

The cyclic voltammograms (CV) for ethanol electro-oxidation, catalyzed by the Ru/Pt/C, Sn/Pt/C and W/Pt/C materials, in 0.1 mol L^{-1} ethanol + 0.5 mol L^{-1} H_2SO_4 solution, which were recorded during repetitive cycling, is presented in Fig. 4(a). The curve obtained for Pt/C was included for comparison. As can be noted, the onset potential of ethanol electro-oxidation obtained for Sn/Pt/C (*ca.* 0.3 V) is lower than those for the other electrocatalysts. Below the onset potential, the reaction seems to be inhibited by adsorbed intermediates such as CO and CH_x species, due to the dissociative adsorption of ethanol. Above 0.5 V, the reaction rate increases considerably due to the oxidation of these adsorbed intermediates. For all investigated materials, it can be observed a double peak in the positive-going scan and, at higher potentials, the current drops due to the competition between the adsorption of ethanol and the activation of water molecules forming Pt—O species. In the negative-going scan, the reaction remains inhibited until the Pt—O electro-reduction at 0.85 V, and then increases abruptly due to the liberation of active metallic Pt sites for ethanol adsorption [22]. After this, the reaction decreases at more negative potentials due to "re-poisoning" of the catalyst surface by CO and CH_x species.

On-line DEMS experiments were utilized for the determination of the ethanol electro-oxidation products. The CO_2 formation was monitored using the $m/z = 22$ signal, which corresponds the doubly ionized molecular ion signal [CO_2^{2+}], and the formation of acetaldehyde was followed at $m/z = 29$, which corresponds to the $[CHO]^+$ fragment [51,52]. The mass signals of the DEMS experiments of potentiodynamic ethanol electro-oxidation, catalyzed by the different investigated materials, are presented in Fig. 5. As can be observed, in the forward scan, the CO_2 signals increase and, then, decrease in the potential interval of high Pt—O coverage.

Table 2
Average current efficiencies (A_q) for CO_2, during ethanol electro-oxidation catalyzed by the different investigated electrocatalysts obtained in 0.1 mol L^{-1} ethanol + 0.1 mol L^{-1} H_2SO_4 solutions, integrated over a complete potential cycle.

Electrocatalyst	K^*_{22}	A_i (CO_2)/CV ethanol 0.1 mol L^{-1}
Sn/Pt/C (1:3)	3.7×10^{-6}	7.4%
Ru/Pt/C (1:3)	3.7×10^{-6}	16.6%
W/Pt/C (1:3)	3.6×10^{-6}	7.3%
W/Pt/C (2:3)	3.8×10^{-6}	–
Pt/C	4.3×10^{-6}	13.0%

Additionally, it can be observed that the onset and magnitude of the CO_2 mass signals follow the trend observed in the CO stripping measurements, indicating similar CO coverage trend, when it is originated from the dissociative adsorption of ethanol. So, the sites for CO adsorption (from dissolved CO) or CO formation (from the C—C bond breaking of ethanol) follow the same order of activity. In the negative-going scan, the CO_2 formation is totally suppressed for all cases. As discussed in previous works [23,53,54], this behavior indicates that the CO_2 formation during the positive-going scan is associated to the oxidation of adsorbed intermediates, such as CO and CH_x, formed from the C—C bond breaking at low potential, to CO_2. The absence of CO_2 in the negative-going scan indicates that the C—C bond break does not take place in higher potentials domain. Furthermore, this can be supported by a previous work [23], where it was suggested that, at low potentials, the rate-determining step is the CO_{ad} oxidation and, at higher potentials, the rate-determining step is the C—C bond breaking (CO_{ad} formation). This explains the formation of CO_2 in the positive-going scan, and its absence in the negative-going scan.

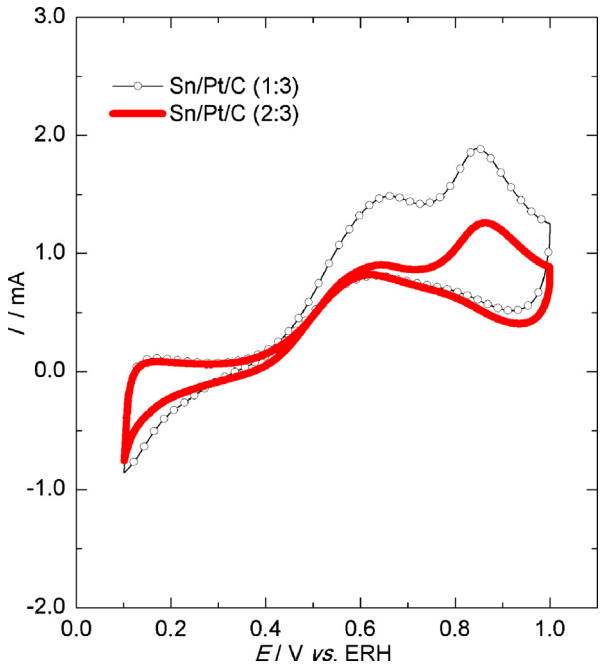

Fig. 7. Faradaic current signals in DEMS measurements obtained during CV of ethanol electro-oxidation catalyzed by Sn/Pt/C (1:3) and Sn/Pt/C (2:3) in 0.1 mol L^{-1} C_2H_5OH and 0.5 mol L^{-1} H_2SO_4 solution at 25 °C and at a scan rate of 10 mV s^{-1}.

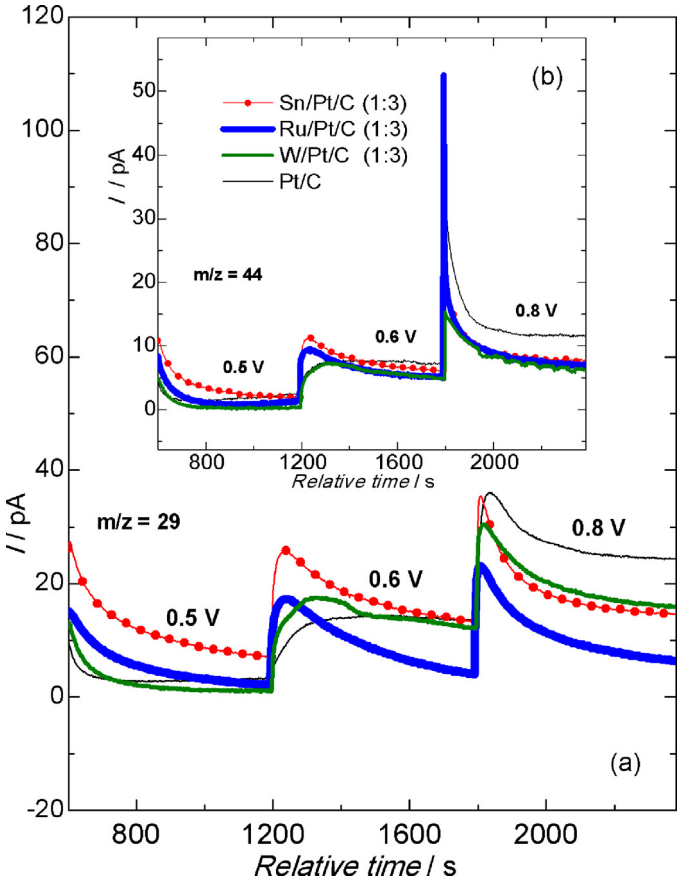

Fig. 6. Ionic currents obtained in DEMS experiments during chronoamperometric measurements of ethanol electro-oxidation reaction catalyzed by the different investigated electrocatalysts: (a) $m/z = 29$ (acetaldehyde, CHO^+), and (b) $m/z = 44$ (CO_2, CO_2^+ + acetaldehyde, CH_3CHO^+) in 0.1 mol L^{-1} ethanol and in 0.5 mol L^{-1} H_2SO_4 electrolyte at 25 °C.

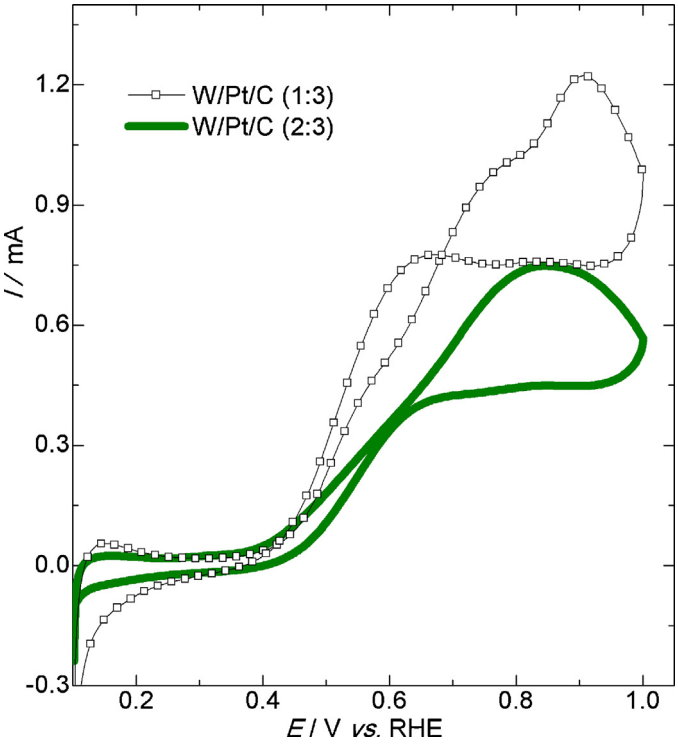

Fig. 8. Ionic currents obtained in DEMS measurements during CV of ethanol electro-oxidation reaction catalyzed by Sn/Pt/C (1:3) and Sn/Pt/C (2:3): (a) $m/z = 22$ (CO_2^{2+}); (b) $m/z = 29$ (acetaldehyde, CHO^+), and (c) $m/z = 44$ (CO_2, CO_2^+ + acetaldehyde, CH_3CHO^+) in 0.1 mol L^{-1} ethanol and in 0.5 mol L^{-1} H_2SO_4 electrolyte at 25 °C. Scan rate of 10 mV s^{-1}.

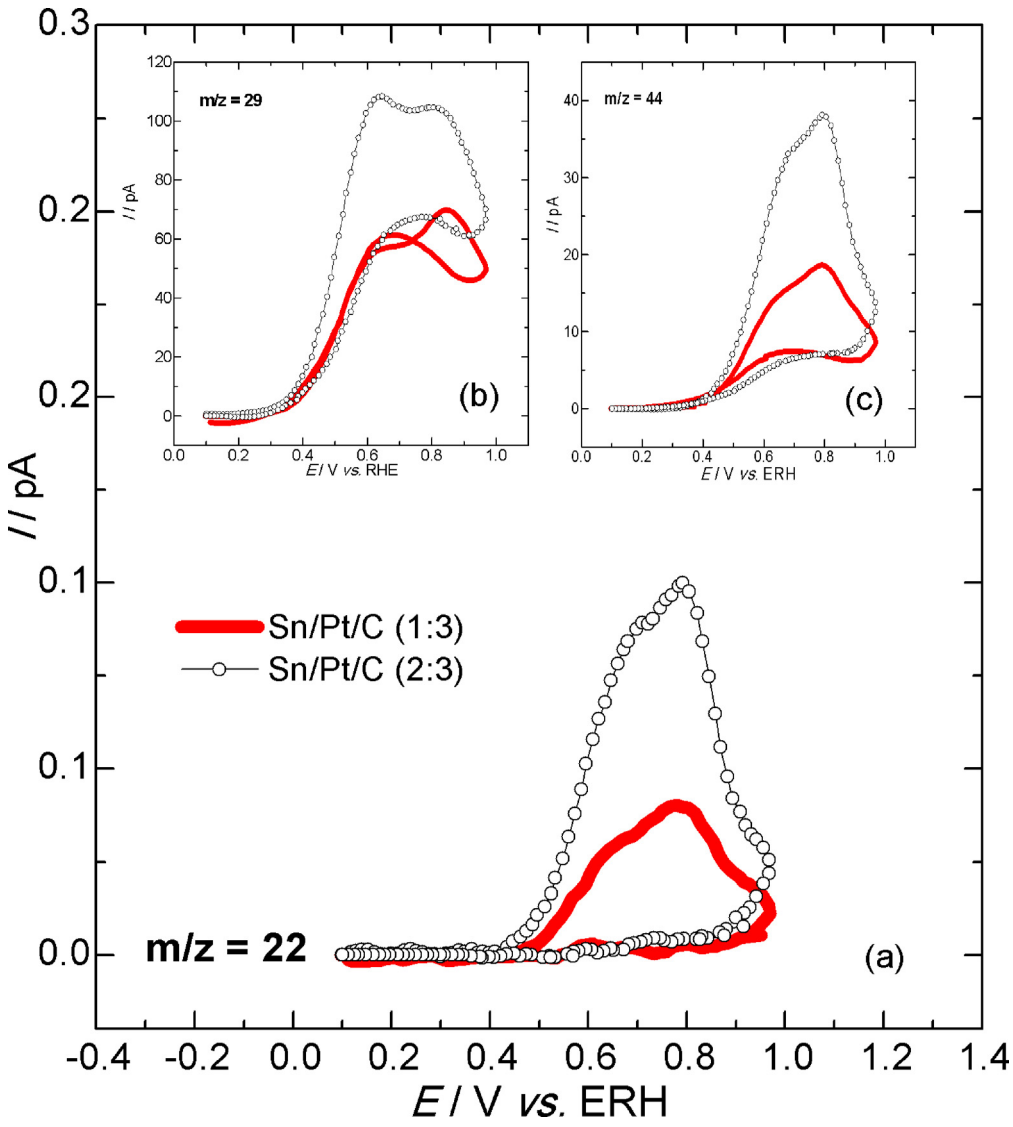

Fig. 9. Faradaic current signals in DEMS measurements obtained during CV of ethanol electro-oxidation catalyzed by W/Pt/C (1:3) and W/Pt/C (2:3) in 0.1 mol L^{-1} C_2H_5OH and 0.5 mol L^{-1} H_2SO_4 solution at 25 °C and at a scan rate of 10 mV s^{-1}.

Analyzing the curves in Fig. 5, it is worth noting that the acetaldehyde signal follows the trend of the Faradaic current of ethanol electro-oxidation. Also, it can be observed that the $m/z = 22$ or $m/z = 44/m/z = 29$ signal ratio is higher for Ru/Pt/C, which indirectly evidences superior current efficiencies for CO_2 formation [55]. In order to make the comparison more quantitative, the average current efficiencies for CO_2 formation were calculated, integrated over a complete voltammogram cycle. (These calculations were used to estimate the trends of CO_2 formation on the different electrocatalysts.) Table 2 presents the results for the different electrocatalysts. It can be noted a higher value for Ru/Pt/C (1:3) (16.6%), this being followed by Pt/C (13.0%), Sn/Pt/C (1:3) (7.4%), and W/Pt/C (1:3) (7.3%). It is important to mention that the high current efficiencies obtained in this work, in comparison to those obtained in the literature [23,45], are due to the use a stagnant electrolyte DEMS cell, and high loading of the electrocatalyst powder in the electrode. The stagnant electrolyte allows the re-adsorption of reaction intermediate species, and the thicker catalytic layer increases the residence time inside the layer, both contributing to increase the conversion efficiency to CO_2. Potentiostatic measurements were also carried out in the same solution for the EOR catalyzed by the different electrocatalysts. The Faradaic currents, presented in Fig. 4(b) (as figure inset), shows a activity trend similar to that obtained in the potentiodynamic measurements, with Sn/Pt/C (1:3) presenting higher currents at 0.5 and 0.6 V (lower onset potential in the CV curves). The $m/z = 29$ and $m/z = 44$ DEMS signals, presented in Fig. 6, also shows that this higher current values, at low potentials, are due to the formation of acetaldehyde, this being a major product. For all cases, a decrease (or deactivation) of the current can be observed, since they drop as a function of the time. This result may be associated to the poisoning of the electrocatalyst surface by adsorbed CO and CH_x species during the course of the EOR. Interestingly, W/Pt/C presented the lowest rate of deactivation, and this is associated to its lower rate or lower activity for the C—C bond dissociation.

DEMS measurements were also conducted in order to investigate the effect of increasing the amount of Sn and W on the reaction product distribution. The obtained results for Sn/Pt/C (see Figs. 7 and 9) show that the increase in the Sn content reduces the Faradaic current of ethanol electro-oxidation, and it is proportionally followed by the $m/z = 22$ (CO_2), 44 (CO_2 and acetaldehyde) and 29 (acetaldehyde) ionic signals. This may be associated to

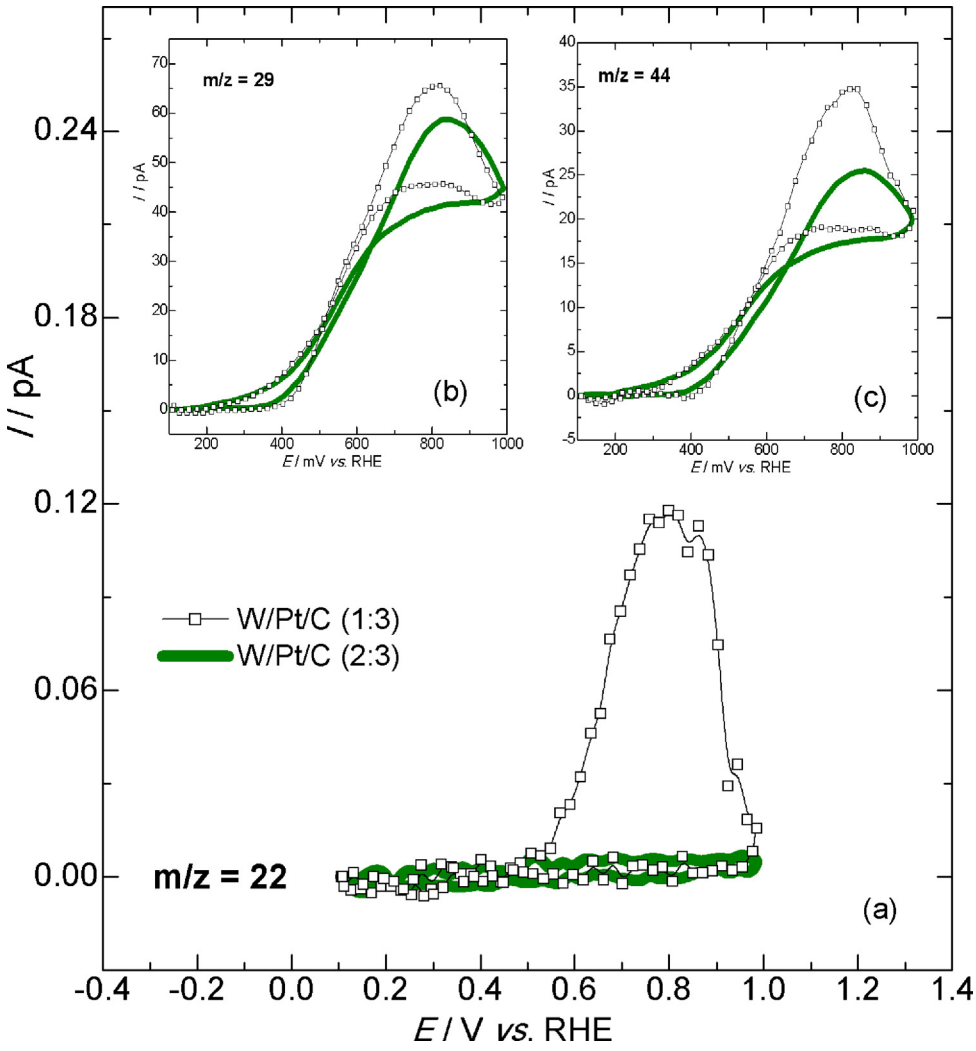

Fig. 10. Ionic currents obtained in DEMS measurements during CV of ethanol electro-oxidation reaction catalyzed by W/Pt/C (1:3) and W/Pt/C (2:3): (a) $m/z = 22$ (CO_2^{2+}); (b) $m/z = 29$ (acetaldehyde, CHO^+), and (c) $m/z = 44$ (CO_2, CO_2^+ + acetaldehyde, CH_3CHO^+) in 0.1 mol L^{-1} ethanol and in 0.5 mol L^{-1} H_2SO_4 electrolyte at 25 °C. Scan rate of 10 mV s^{-1}.

the diminished number of Pt sites that are active for the EOR, and to an increase in the Sn content on the nanoparticle surface, that are active only for the water activation (or water breaking). Accordingly, as the Faradaic current of ethanol electro-oxidation is proportionally followed by the CO_2 and acetaldehyde mass signals, it can be assumed that the proportion between the C_1 and C_2 parallel pathways of the EOR is unaltered with the variation of the Sn content.

On the other hand, an important result was obtained due to alteration in the W content in the W/Pt/C electrocatalyst. As can be observed in Figs. 8 and 10, the increase in the W content is accompanied by a decrease of the EOR Faradaic current, and this is followed by a decrease in the $m/z = 29$ ionic signal. However, this decrease in the Faradaic current is not proportionally accompanied by the $m/z = 22$ and $m/z = 44$ signals. Indeed, the mass signal for CO_2 ($m/z = 22$) is completely suppressed (or at least undetectable) for the electrocatalyst with high W content (this results in an average Faradaic current efficiency for CO_2 formation equal to zero). As mentioned above, the ethanol electro-oxidation reaction may involve steps of ethanol adsorption, deprotonation, C—C bond breaking, and oxygen addition to form CO_2. So, on W/Pt/C (2:3) electrocatalyst, it seems that the steps of adsorption and deprotonation, forming adsorbed hydrogen, still occur, but the formation of reactive species such as CH_2CHO_{ads} or $CH_2CH_2O_{ads}$, suggested in the Ref. [32], may not take place, inhibiting or decelerating the C—C bond breaking step. The inhibition of the C—C bond breaking can also be indirectly evidenced by the absence of the $m/z = 15$ ionic signal, which corresponds to methane formation (not shown here for brevity). Mainly for Pt/C and Ru/Pt/C, the formation of methane was observed at lower potential domains due to the electro-reduction of adsorbed species with one carbon, such as CH_x and CO. Therefore, the non-detection of methane for W/Pt/C (2:3) indirectly evidences the non-occurrence of the ethanol dissociative adsorption on the surface of this electrocatalyst (or, at least, to an insignificant rate of dissociation). Furthermore, potentiostatic measurements of the EOR, catalyzed by W/Pt/C (2:3), showed much lower deactivation in comparison to that for W/Pt/C (1:3) (not shown here for brevity). This also confirms the non-occurrence (or very low rate) of the C—C bond breaking on this material, inhibiting the formation of the poisoning CO or CH_x species.

Additionally, the activity of the W/Pt/C (2:3) electrocatalyst for the acetaldehyde electro-oxidation was investigated. Fig. 11 shows the cyclic voltammograms for acetaldehyde electro-oxidation catalyzed by the W/Pt/C (2:3) and Pt/C materials in 0.1 mol L^{-1} acetaldehyde + 0.5 mol L^{-1} H_2SO_4 solution, which were recorded during repetitive cycles in DEMS experiments. The curves for the electro-oxidation of ethanol on both materials were added for comparison. As can be noted, Pt/C is active for ethanol and for

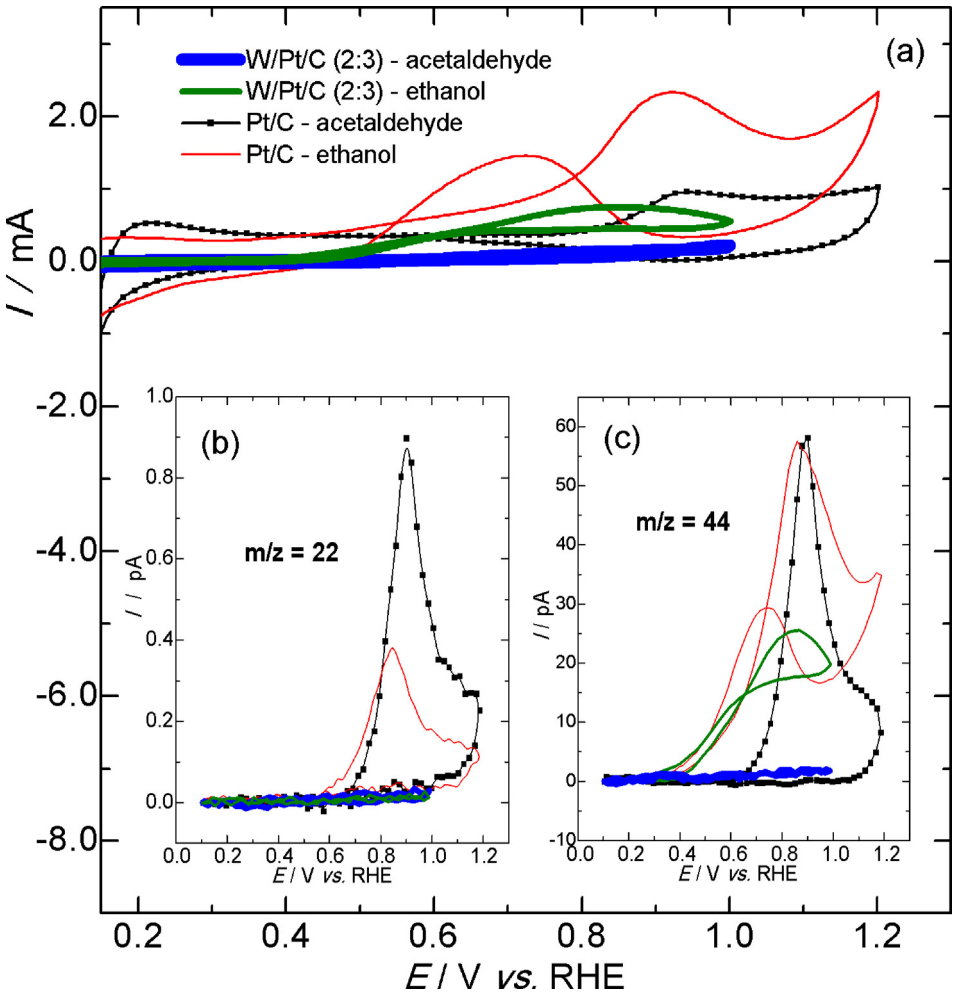

Fig. 11. Faradaic current (a) and ionic current signals of $m/z = 22$ (b) and $m/z = 44$ (c) obtained during cyclic voltammetry in during DEMS measurements of acetaldehyde and ethanol electro-oxidation catalyzed by W/Pt/C (2:3) and Pt/C in 0.1 mol L^{-1} CH_3CHO or CH_3CH_2OH and 0.5 mol L^{-1} H_2SO_4 solution at 25 °C and at a scan rate of 10 mV s^{-1}.

acetaldehyde electro-oxidation, and the CO_2 formation is clearly seen for both cases (Fig. 11(b) and (c)). For the W/Pt/C (2:3) electrocatalyst, it can be noted a Faradaic current for the EOR, but with no CO_2 formation, as previously presented in Fig. 10. On the other hand, this material was non-active for the acetaldehyde electro-oxidation (absence of Faradaic current) and, as a consequence, there is no signal for CO_2. Therefore, it can be stated that the W/Pt/C (2:3) material is inactive for the C—C bond breaking in ethanol molecule, and totally inactive for acetaldehyde electro-oxidation. The electro-oxidation of ethanol and its intermediate products on Pt-based materials were also investigated by other researchers, and can be encountered in previous published works, with interesting results [56,57].

3.3. RDE experiments of the HOR catalyzed by W/Pt/C

Considering the presented results, in a practical point of view, as W/Pt/C (2:3) was inactive for acetaldehyde, and this molecule can be a dehydrogenation by-product of ethanol, the W/Pt/C (2:3) material was investigated as electrocatalyst for the hydrogen electro-oxidation reaction in the absence and in the presence of acetaldehyde in the electrolyte. For both electrocatalysts, the RDE curves, obtained at different rotation rates, showed that the limiting current crosses the origin and linearly increases with the square root of the rotation rate, suggesting that the limiting current is diffusion controlled (not shown) [40,58–60]. Fig. 12 shows the experimental RDE curves obtained at 1600 rpm (linear scan (a), and chronoamperometric curves at 0.1 V (b)) for the HOR catalyzed by W/Pt/C (2:3) and Pt/C (included for comparison). The analysis of the RDE at 1600 rpm and the chronoamperometric curves reveals superior electrocatalytic activity of Pt/C. According to "volcano" plots for the hydrogen oxidation or evolution reaction, Pt is more active than W [61] and, therefore, Pt/C seems to be more active than W/Pt/C (2:3) for HOR due to its higher number of Pt atoms in the particle surface and due to a non-beneficial electronic effect of W on the Pt d-band. In the presence of acetaldehyde in the electrolyte, Pt/C showed a significant decrease in the RDE and in the chronoamperometric anodic currents. W/Pt/C (2:3) presented a slight decrease in the current for the RDE and only a marginal decrease for the potentiostatic measurement. This result may be ascribed to the poisoning of the Pt/C surface due to the dissociative adsorption of acetaldehyde molecules, producing adsorbed CO and CH_x species, which do not suffer eletro-oxidation at potentials lower than *ca.* 0.75 V. W/Pt/C (2:3) has lower activity for the HOR but, on the other hand, does not show significant deactivation due to its inactivity for the C—C bond breaking and, so, excluding the formation of undesired CO and CH_x species on its surface. Therefore, W/Pt/C (2:3) would be an interesting candidate as electrocatalyst of the anode of indirect hydrogen fuel cells operating with ethanol. The coupling of an ethanol dehydrogenation reactor with an indirect hydrogen fuel cell is in development in the laboratory.

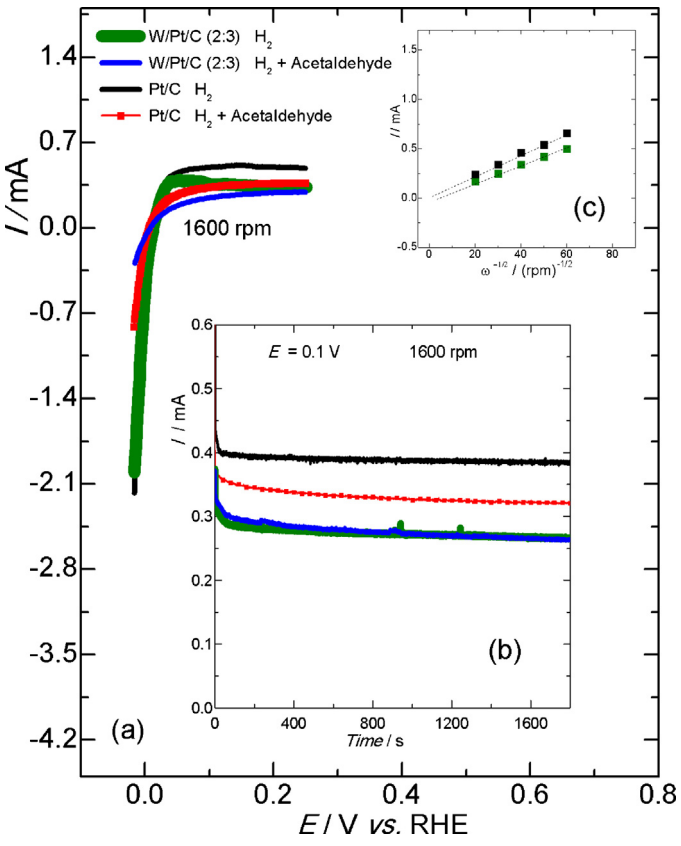

Fig. 12. Faradaic currents obtained during (a) cyclic voltammetry and (b) chronoamperometry in RDE measurements of H_2 or H_2 + 0.1 mol L^{-1} CH_3CHO electro-oxidation catalyzed by W/Pt/C (2:3) and Pt/C in 0.5 mol L^{-1} H_2SO_4 electrolyte at 25 °C. The CV measurements were conducted at a scan rate of 10 mV s^{-1} and the chronoamperometric curves were performed at E = 0.1 V during 30 min. Rotating rate of 1600 rpm.

4. Conclusions

The results obtained in this work showed that Ru/Pt/C and Sn/Pt/C presented higher overall reaction rate than Pt/C at lower overpotentials, but were non-selective for the C_1 or C_2 pathways, catalyzing the reaction producing CO_2 and acetaldehyde in parallel pathways. Ru/Pt/C presented the highest average current efficiency for CO_2 formation with the value of 16.6%. The increase in the Ru or Sn content did not change significantly the proportion between CO_2 and acetaldehyde. Nevertheless, W/Pt/C, with high W content (2:3), was selective to the C_2 route. Additionally, W/Pt/C (2:3) was practically inactive for acetaldehyde electro-oxidation and more active and stable for H_2 electro-oxidation in the absence and in the presence of acetaldehyde, contrarily to what was observed for Pt/C. This was attributed to its ability for H_2 electro-oxidation and its inability for the C—C bond breaking, which inhibited the formation of the poisoning CO and CH_x adsorbed species. Considering that W/Pt/C, with high amount of W, is active of the H_2 electro-oxidation and it is selective for the ethanol and acetaldehyde electro-oxidation *via* the C_2-pathway, in a practical point of view, this material could be used as the anode electrocatalyst of indirect hydrogen fuel cells, mainly for those that operates as auxiliary power units of internal combustion engine cars.

Acknowledgments

The authors gratefully acknowledge financial support from the FAPESP (*Fundação de Amparo à Pesquisa do Estado de São Paulo* – São Paulo Research Foundation) – F.H.B.L. – Grant No 2009/07629-6, 2008/05156-0, and 2011/50727-9, and A.C.Q. – Grant No: 2013/00197-9, CNPq (*Conselho Nacional de Desenvolvimento Científico e Tecnológico*) – F.H.B.L. – Grant No: 306213/2013-3, and CAPES (*Coordenação de Aperfeiçoamento de Pessoal de Nível Superior*) for financial support.

References

[1] D.U. Eberle, D.R. von Helmolt, Energy Environ. Sci. 3 (2010) 689–699.
[2] U. Eberle, M. Felderhoff, F. Scheuth, Angew. Chem. Int. Ed. 48 (2009) 6608–6630.
[3] F. Crotogino, S. Donadei, U. Bunger, H. Landinger, Large-Scale Hydrogen Underground Storage for Securing Future Energy Supplies, Essen, Germany, 2010, May 16–21.
[4] A.M. Ozerova, O.A. Bulavchenko, O.V. Komova, O.V. Netskina, V.I. Zaikovskii, G.V. Odegova, V.I. Simagina, Kinet. Catal. 53 (2012) 511–520.
[5] O. Akdim, U.B. Demirci, P. Miele, Int. J. Hydrogen Energy 36 (2011) 13669–13675.
[6] S.K. Green, G.A. Tompsett, H.J. Kim, W.B. Kim, G.W. Huber, ChemSusChem 5 (2012) 2410–2420.
[7] C. Lamy, A. Devadas, M. Simoes, C. Coutanceau, Electrochim. Acta 60 (2012) 112–120.
[8] C.M. Araujo, D.L. Simone, S.J. Konezny, A. Shim, R.H. Crabtree, G.L. Soloveichik, V.S. Batista, Energy Environ. Sci. 5 (2012) 9534–9542.
[9] P.F. Driscoll, E. Deunf, L. Rubin, O. Luca, R. Crabtree, C. Chidsey, J. Arnold, J.B. Kerr, ECS Trans. 35 (28) (2011) 3–17.
[10] N. Kariya, A. Fukuokaa, M. Ichikawa, Phys. Chem. Chem. Phys. 8 (2006) 1724–1730.
[11] W. Vielstich, H.A. Gasteiger, A. Lamm, Handbook of Fuel Cells: Fundamentals, Technology and Applications, 4, Willey, Weinheim, 2003.
[12] S.M. Lima, R.C. Colman, G. Jacobs, B.H. Davis, K.R. Souza, A.F.F. Lima, L.G. Appel, L.V. Mattos, F.B. Noronha, Catal. Today 146 (2009) 110–123.
[13] A. Neramittagapong, W. Attaphaiboon, S. Neramittagapong, Chiang Mai J. Sci. 35 (1) (2008) 171–177.
[14] A.G. Sato, D.P. Volanti, D.M. Meira, S. Damyanov, E. Longo, J.M.C. Bueno, J. Catal. 307 (2013) 1–17.
[15] A.G. Sato, D.P. Volanti, I.C. de Freitas, E. Longo, J.M.C. Bueno, Catal. Commun. 26 (2012) 122–126.
[16] S.C. Zignani, V. Baglio, J.J. Linares, G. Monforte, E.R. Gonzalez, A.S. Arico, Int. J. Hydrogen Energy 38 (2013) 11576–11582.
[17] T.S. Almeida, L.M. Palma, C. Morais, K.B. Kokoh, A.R. De Andrade, J. Electrochem. Soc. 160 (9) (2013) F965–F971.
[18] G. Andreadis, V. Stergiopoulos, S. Song, P. Tsiakaras, Appl. Catal. B: Environ. 100 (2010) 157–164.
[19] N. Kariya, A. Fukuokaa, M. Ichikawa, Chem. Commun. 690 (2003) 690–691.
[20] S.C.S. Lai, S.E.F. Kleijn, F.T.Z. Ozturk, V.C. van Rees Vellinga, J. Koning, P. Rodriguez, M.T.M. Koper, Catal. Today 154 (2010) 92–104.
[21] V. Del Colle, J. Souza-Garcia, G. Tremiliosi-Filho, E. Herrero, J.M. Feliu, Phys. Chem. Chem. Phys. 13 (2011) 12163–12172.
[22] T. Iwasita, E. Pastor, Electrochim. Acta 39 (4) (1994) 531–537.
[23] H. Wang, Z. Jusys, R.J. Behm, J. Power Sources 154 (2006) 351–359.
[24] D.A. Cantane, W.F. Ambrosio, M. Chatenet, F.H.B. Lima, J. Electroanal. Chem. 681 (2012) 56–65.
[25] C. Lamy, A. Lima, V. LeRhum, F. Delime, C. Coutanceau, J.-M. Leger, J. Power Sources 105 (2002) 283–296.
[26] H.F. Wang, Z.P. Liu, J. Am. Chem. Soc. 130 (2008) 10996–11004.
[27] J. Souza-Garcia, E. Herrero, J.M. Feliu, ChemPhysChem 11 (2010) 1391–1394.
[28] F. Colmati, G. Tremiliosi-Filho, E.R. Gonzalez, A. Berna, E. Herrero, J.M. Feliu, Faraday Discuss. 140 (2008) 379–397.
[29] F.H.B. Lima, D. Profeti, W. Lizcano-Valbuena, E.A. Ticianelli, E.R. Gonzalez, J. Electroanal. Chem. 617 (2008) 121–129.
[30] W.P. Zhou, S. Axnanda, M.G. White, R.R. Adzic, J. Hrbek, J. Phys. Chem. C 115 (2011) 16467–16473.
[31] E. Antolini, J. Power Sources 170 (2007) 1–12.
[32] A. Kowal, M. Li, M. Shao, K. Sasaki, M.B. Vukmirovic, J. Zhang, N.S. Marinkovic, P. Liu, A.I. Frenkel, R.R. Adzic, Nat. Mater. (2009) 325–330.
[33] D.M. dos Anjos, F. Hahn, J.-M. Leger, K.B. Kokoha, G. Tremiliosi-Filho, J. Braz. Chem. Soc. 19 (2008) 795–802.
[34] X. He, C. Hu, Q. Yi, X. Wang, H. Hua, X. Li, J. Electrochem. Soc. 160 (6) (2013) F566–F572.
[35] R.C.H. Maya, O.U. Reyes, J.G. Fadrique, H.C. Lopez, P.R. Tejeda, J. Electrochem. Soc. 160 (3) (2013) H185–H191.
[36] K. Miecznikowski, J. Solid State Electrochem. 16 (2012) 2723–2731.
[37] W. Zhou, Z. Zhou, S. Song, W. Li, G. Suna, P. Tsiakaras, Q. Xin, Appl. Catal. B: Environ. 46 (2003) 273–285.
[38] S. Sao-Joao, S. Giorgio, J.M. Penisson, C. Chapon, S. Bourgeois, C. Henry, J. Phys. Chem. B 109 (2005) 342–347.
[39] A.R. West, Solid State Chemistry and Its Applications, Wiley, New York, 1984.
[40] T.J. Schmidt, H.A. Gasteiger, G.D. Stab, P.M. Urban, D.M. Kolb, R.J. Behm, J. Electrochem. Soc. 145 (1998) 2354–2358.
[41] J.P.I. de Souza, S.L. Queiroz, F.C. Nart, Quim. Nova 23 (3) (2000) 384–391.
[42] B. Bittins-Cattaneo, E. Cattaneo, P. Konigshoven, W. Vielstich, in: A.J. Bard (Ed.), Electroanalytical Chemistry – A Series of Advances, vol. 17, Marcel Dekker, New York, 1991, p. 181.
[43] R. Ianniello, V.M. Ber Schmidt, Bunsen-Ges. Phys. Chem. 99 (1995) 83–99.

[44] L. Jiang, L. Colmenares, Z. Jusys, G.Q. Sun, R.J. Behm, Electrochim. Acta 53 (2007) 377–389.
[45] V. Rao, C. Cremers, U. Stimming, L. Cao, S. Sun, S. Yan, G. Sun, Q. Xin, J. Electrochem. Soc. 154 (2007) B1138–B1147.
[46] C. Cremers, B. Kintzel, D. Bayer, J. Tubke, ECS Trans. 33 (2010) 1681–1692.
[47] J.P.I. Souza, T. Iwasita, F.C. Nart, W. Vielstich, J. Appl. Electrochem. 30 (1999) 43–48.
[48] M. Watanabe, S. Motoo, J. Electroanal. Chem. 60 (1975) 267–273.
[49] F.H.B. Lima, E.R. Gonzalez, J. Appl. Catal. B: Environ. 79 (2008) 341–346.
[50] F.H.B. Lima, D. Profeti, M. Chatenet, D. Riello, E.A. Ticianelli, E.R. Gonzalez, Electrocatalysis 1 (2010) 72–82.
[51] H. Wang, Z. Jusys, R.J. Behm, J. Phys. Chem. B 108 (2004) 19413–19424.
[52] A.A. Abd-El-Latifa, E. Mostafa, S. Huxter, G. Attard, H. Baltruschat, Electrochim. Acta 55 (2010) 7951–7960.
[53] S. Sun, M. Chojak Halseid, M. Heinen, Z. Jusys, R.J. Behm, J. Power Sources 190 (2009) 2–13.
[54] Z. Jusys, J. Kaiser, R.J. Behm, Langmuir 19 (2003) 6759–6769.
[55] F.H.B. Lima, E.R. Gonzalez, J. Electrochim. Acta 53 (2008) 2963–2971.
[56] Y. Wang, S. Song, G. Andreadis, H. Liu, P. Tsiakaras, J. Power Sources 196 (2011) 4980–4986.
[57] S. Song, C. He, J. Liu, Y. Wang, A. Brouzgou, P. Tsiakaras, Appl. Catal. B: Environ. 119–120 (2012) 227–233.
[58] P.S. Ruvinsky, S.N. Pronkin, V.I. Zaikovskii, P. Bernhardta, E.R. Savinova, Phys. Chem. Chem. Phys. 10 (2008) 6665–6676.
[59] A. Bonnefont, A.N. Simonov, S.N. Pronkin, E.Yu. Gerasimov, P.A. Pyrjaev, V.N. Parmon, E.R. Savinova, Catal. Today 202 (2013) 70–78.
[60] M. Shao, J. Power Sources 196 (2011) 2433–2444.
[61] J.K. Nørskov, T. Bligaard, A. Logadottir, J.R. Kitchin, J.G. Chen, S. Pandelov, U. Stimming, J. Electrochem. Soc. 152 (3) (2005) J23–J26.